Non-Monotonic γ-Ray Influence on Mo/n-Si Schottky Barrier Structure Properties

Oleg Ya. Olikh

***Abstract*—The current-voltage characteristics of Mo/n-Si Schottky barrier structure irradiated by γ-rays of ^{60}Co were investigated in the temperature range of 120–330 K. The zero-bias barrier height, ideality factor, and reverse current were found to depend non-monotonously on the cumulative dose. The samples exposed to different radiation doses were found to display different forward current transport mechanism. In non-irradiated structure the current-transport mechanism is thermionic emission (TE) over inhomogeneous barrier. In the structure exposed to 10 kGy the mechanism is defect-assisted tunneling in the lower temperature range 120–220 K, and TE over inhomogeneous barrier in the higher temperature range 260–330 K. In the structure exposed to 100 kGy the mechanism is tunneling in the 150–220 K range, and TE (dominant) and tunneling at 260–330 K. The obtained results are explained by the increase of radiation defect concentrations (for comparatively small doses), and by further gettering of defects in the inhomogeneous regions as the irradiation dose increases.**

***Index Terms*—Dose rate effects, gamma-ray effects, semiconductor devices, silicon.**

I. Introduction

THE electrical characteristics of metal-semiconductor (MS) contact are known to be extremely sensitive to the density of states at MS interface. Therefore, any factor capable of changing the interface state influences the characteristics of Schottky diodes (SDs) as well. One of the most widespread external effects is radiation. The structures with Schottky contacts are widely used in microwave FETs, RF detectors, solar cells and so on; they are also widely applied in high-speed logic circuits, integrated and optoelectronic technologies. Since the semiconductor devices often operate under various irradiation conditions, for example, in space, the studies of irradiation impact on MS structure become increasingly important. They would provide not only better understanding of radiation-solid interaction at the interface but also the fundamental knowledge for practical applications.

The research in this field has received much attention in recent years [1]–[15]. In particular, there are reliable data about monotonic decrease of barrier height as well as monotonic increase of ideality factor and reverse current in Schottky barrier (SB) structures with n-type semiconductor exposed to ion and electron irradiation [1]–[5]. These effects arise from radiation-induced defects, which leads to the change the concentration of free carriers and increase the density of states at the interface which in turn causes tunneling current enhancement. At the same time Schottky barrier height (SBH) increase and ideality factor decrease are often observed in the samples exposed to γ-radiation regardless of the semiconductor material or of the type of conductivity [6]–[8]. The mechanism proposed to explain these effects is charge compensation and intensification of defect-assisted tunneling (DAT) via radiation-induced defects at the interface [8]. However, the researchers also report about the decrease of SBH after exposition to γ-radiation [9]. Moreover, when estimated by current-voltage *(I-V)* characteristics, the SBH has been found to depend non-monotonically on the absorbed dose of ^{60}Co γ-radiation [10], [11]. This non-monotonic dose dependence of electrical parameters has been revealed not only for SD exposed to γ-rays, but also for various barrier structures [12] or/and types of radiation [13]–[15]. It should be noted that non-monotonic dose dependences observed in MS structures are of different kinds: for example, SBH has been shown to increase at a low dose and to decrease at a high dose of irradiation [10], [13], [14] whereas in [11] an opposite dependence is described. Nevertheless, the causes of these contradictions have not been duly explained so far.

In recent years, however, a number of attempts have been made to account for a wide range of observed *I-V* characteristics by applying inhomogeneous SB concept [16]–[21]. There are two theories that are widely used within this paradigm [16]: the first theory proposes to use interacting Gaussian distribution of SBH to account for spatial inhomogeneities [22]; the second theory relies on a patchwork of low barrier regions embedded in the homogeneous high barrier region [23]. Besides, an attempt has been made to combine both these theories in one approach [20], [21].

The aim of our work is to study non-monotonic dose dependence of SD parameters in detail. For this purpose we have measured *I-V* characteristics of Mo/n-Si Schottky barrier structure exposed to different doses of ^{60}Co γ-rays in a wide range of temperatures. The radiation dose was chosen basing on data from [10] where the silicon structure SBH was found to increase at ^{60}Co γ-ray cumulative dose $D_\gamma \approx 10$ kGy and subsequently to decrease with growing D_γ up to 100 kGy. The results have been analyzed by using inhomogeneous SB paradigm.

II. Experimental and Calculation Details

The samples used in our experiments were 0.2 μm thick n-Si:P epitaxial layer on $n^+ - Si:Sb$. The thickness of the substrate was 250 μm and the free carrier concentration in

Manuscript received June 27, 2012; revised October 01, 2012; accepted December 05, 2012. Date of publication January 30, 2013; date of current version February 06, 2013.

The author is with the Faculty of Physics, Taras Shevchenko Kyiv National University, Kyiv 01601, Ukraine (e-mail: olikh@univ.kiev.ua).

Color versions of one or more of the figures in this paper are available online at http://ieeexplore.ieee.org.

Digital Object Identifier 10.1109/TNS.2012.2234137

it was 4.2×10^{22} m^{-3}. The molybdenum Schottky junction fabricated on the epi-layer surface was 2 mm in diameter.

The investigated structures were exposed to ^{60}Co γ-ray radiation. The cumulative doses were 10 kGy and 100 kGy for the samples labeled M10 and M100 respectively. The non-irradiated sample was labeled M0. The capacitance-voltage characteristics were measured at room temperature. These measurements showed that the epi-layer carrier concentrations N_d were 1.15×10^{23}, 1.10×10^{23} and 1.19×10^{23} m^{-3} for M0, M10, and M100 respectively.

The forward and reverse *I-V* characteristics were measured in dc current from 10^{-9} to 2×10^{-2} A in the temperature range from 120 to 330 K. The sample temperature was controlled by a differential copper-constantan thermocouple.

The SD forward current can be expressed as [24]–[26]:

$$I = I_S \exp\left(\frac{q(V - IR_S)}{nkT}\right)\left[1 - \exp\left(-\frac{q(V - IR_S)}{kT}\right)\right] \quad (1)$$

where V is the forward bias, I_S is the saturation current, n is the ideality factor, R_S is the series resistance. To deduce R_S we used Gromov's method [26] and plotted the dependence of $\ln(I/\{1 - exp[-q(V - IR_S)/(kT)]\})$ on V to obtain I_S and n from *I-V* data. The slope and intercept of the plot provide ideality factor and saturation current respectively.

III. Results and Discussion

Fig. 1 shows the *I-V* characteristics measured for Mo/n-Si structures at different temperatures. It can be seen that the forward current has two components: the first is the main component that dominates at $I > 10^{-5}$ A, and the second is the additional component prevailing at $I < 5 \times 10^{-7}$ A. The series resistance (especially for M0 and M100) has considerable influence on the *I-V* characteristic of the second component, whereas $\log(I) - V$ characteristic of the main component is close to a straight line. Therefore, the following expression can be used to approximate the forward *I-V* characteristic:

$$I = I_1 + I_2 = I_{S1} \exp\left(\frac{qV}{n_1 kT}\right) \cdot \left[1 - \exp\left(-\frac{qV}{kT}\right)\right] + I_{S2} \exp\left(\frac{q(V - IR_S)}{n_2 kT}\right) \times \left[1 - \exp\left(-\frac{q(V - IR_S)}{kT}\right)\right] \quad (2)$$

where I_1 and I_2 are the main and additional component respectively. The above procedure was used to obtain I_{S1}, n_1 and I_{S2}, n_2, R_S from *I-V* characteristics at $I > 10^{-5}$ A and at $I < 5 \times 10^{-7}$ A respectively.

The obtained results are presented in Figs. 2 and 3. It can be seen that non-monotonic dose dependence is observed for ideality factor and saturation current. In particular, i) n_1 for M10 is larger than that for M0 in the measured temperature range, whereas n_1 for M100 is smaller than n_1 for M10 at $T > 190$ K and n_1 for M0 at $T > 260$ K (Fig. 2); ii) the M10 saturation current of the main component is larger than that for M0, whereas I_{S1} decreases with the dose increase, and the M100 current is smaller than the M0 current at $T > 220$ K [Fig. 3(a)]; iii) the

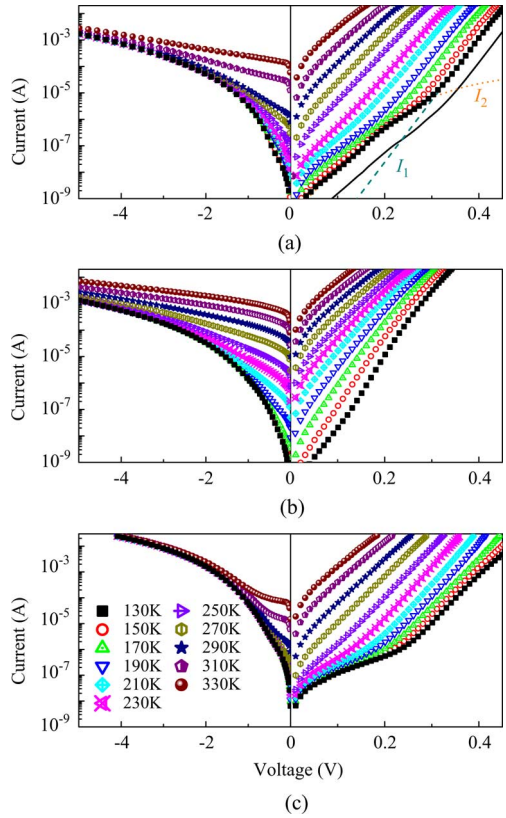

Fig. 1. The forward *I-V* characteristics as a function of temperature for Mo/n-Si Schottky contacts. D_γ, kGy: 0 (a), 10 (b), 100 (c). The full line is the fitting to the *I-V* characteristics at $T = 130$ K calculated by using (2) with $n_1 = 1.67$, $n_2 = 2.53$, $I_{S1} = 4.1 \times 10^{-13}$ A, $I_{S2} = 3.8 \times 10^{-10}$ A, $R_S = 4.1 \times 10^3$ Ohm; the dashed and dotted lines are the main and additional current components I_1 and I_2 respectively.

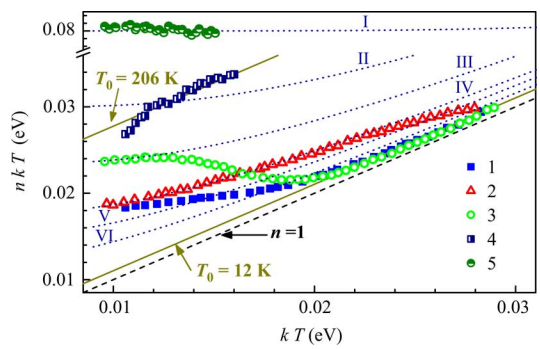

Fig. 2. The temperature dependences of inverse slope of the main (1–3) and additional (4–5) current components. D_γ, kGy: 0 (1, 4), 10 (2), 100 (3, 5). The marks are the experimental results. The full lines are calculated by using (5) with $T_0 = 12$ and 206 K. The dotted lines are calculated by using (14) with E_{00}, meV: 80 (I), 30 (II), 23.5 (III), 17.8 (IV), 15 (V), 12 (VI). The dashed line is ideal case $n = 1$.

low dose leads to the decrease of the additional component saturation current whereas increase in I_{S2} is observed at a higher dose [Fig. 3(b)].

It is known that the flow of carriers over SB can be due to different current-transport mechanisms such as thermionic emission (TE), thermal field emission (TFE), tunneling, DAT, carrier generation and recombination, etc. The non-monotonic dose dependences could be related to the change of current-transport

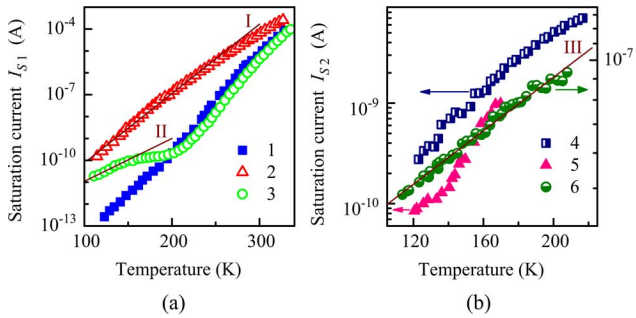

Fig. 3. The temperature dependences of saturation current of the main (a) and additional (b) current components. D_γ, kGy: 0 (1, 4), 10 (2, 5), 100 (3, 6). The full lines are calculated by using (16). χ, 10^{-3} K^{-1}: 73 (I), 42 (II), 26 (III) and I_S, A: 5×10^{-14} (I), 1.3×10^{-13} (II), 1.7×10^{-8} (III).

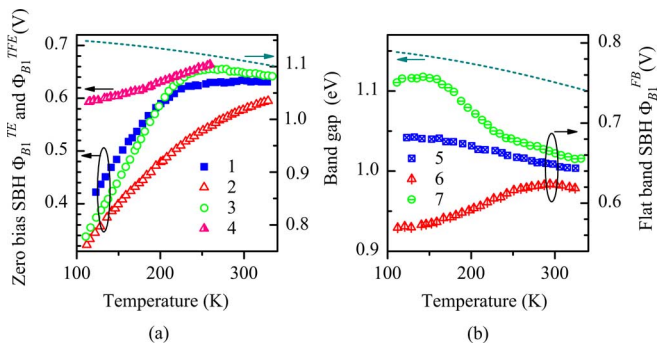

Fig. 4. The temperature dependences of TE zero bias SBH (1, 2, 3), TFE zero bias SBH (4) and flat band SBH (5, 6, 7) of the main current component. D_γ, kGy: 0 (1, 5), 10 (2, 4, 6), 100 (3, 7). The dashed line is the temperature dependence of band gap energy.

mechanism after irradiation. Thus, further we shall consider different possible mechanisms for the structures under study.

A. Thermionic Emission

The relationship between I_S and zero bias SBH Φ_B^{TE} is expressed in terms of the TE theory [24]

$$\Phi_B^{TE} = \left(\frac{kT}{q}\right) \cdot \ln\left(\frac{AA^*T^2}{I_S}\right) \tag{3}$$

where A is the diode area, A^* is the effective Richardson constant of 112 A $\cdot$ cm^{-2}K^{-2} for n-Si [27]. The temperature dependences of Φ_{B1}^{TE} calculated by using experimental I_{S1} values for the main current component are shown in Fig. 4(a). It should be noted that Φ_B^{TE} decreases at low cumulative dose and increases at a higher dose. A similar result is presented in [11]. The zero bias SBH is well known from [24]

$$\Phi_B = \gamma_1(\Phi_m - \zeta) + (1-\gamma_1)\left[\left(\frac{E_g}{q}\right) - \varphi_0\right] - \Delta\Phi_{im} \tag{4}$$

where $\gamma_1 = 1/[1 + q\delta D_s/(\varepsilon_s\varepsilon_0)]$, Φ_m is the metal work function, ζ is the electron affinity of the semiconductor, E_g is the energy band gap of semiconductor, φ_0 is the neutral level of the interface states, $\Delta\Phi_{im}$ is the barrier lowering due to the image force, δ is the oxide layer thickness, D_s is the interface state density, ε_s is the dielectric constant of Si. Therefore, SBH is expected to decrease with increasing the temperature by a coefficient which is approximately equal to the temperature dependence of E_g. Such dependence was also observed experimentally for real structures with a homogeneous SB [28], [29]. The temperature dependence of E_g calculated by using $E_g = 1.17 - 4.73 \cdot 10^{-4}T^2/(T + 636)$[30] is shown in Fig. 4. Similar behavior is observed only for M100 at $T > 260$ K [Fig. 4(a), curve 3].

The ideality factor temperature dependence for TE case is often described as follows:

$$n = 1 + \frac{T_0}{T} \tag{5}$$

where T_0 is a constant which is independent of temperature and bias over a wide temperature range [24], [25]. As seen from Fig. 2, the experimental dependence $n_1(T)$ for M100 is sufficiently well described by (5) with $T_0 = 12$ K at $T > 260$ K.

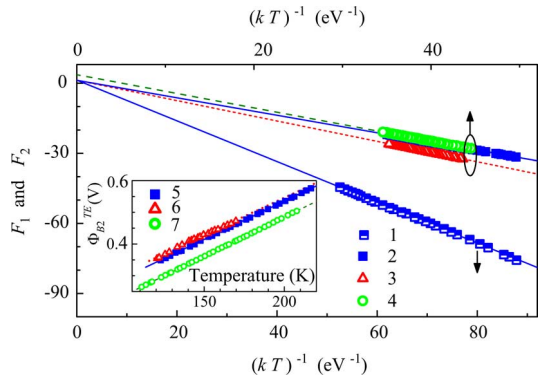

Fig. 5. The modified (1–3) and conventional (4) Richardson plots. The plots are calculated for the main current component in temperature range of 120–220 K (1), 230–330 K (2), 260–330 K (3, 4). σ_Φ, $\times 10^{-3}$ V: 40 (1), 99 (2), 100 (3). Inset shows the temperature dependence of SBH, calculated by using (3) for the additional current component. The lines are the least-squares linear fitting (full for M0, dotted for M10, dashed for M100). D_γ, kGy: 0 (1, 2, 5), 10 (3, 6), 100 (4, 7).

Therefore, the TE mechanism is appropriate for describing the main current component in M100 at $T > 260$ K.

Besides, SBH and A^* can be obtained by using the Richardson plot (the dependence of $F_1 = \ln(I_S/T^2)$ on $(kT)^{-1}$) [24], [27]. According to (3), the slope and intercept of the plot yield Φ_B and Richardson constant respectively

$$F_1 = \ln\left(\frac{I_S}{T^2}\right) = \ln(AA^*) - \frac{q\Phi_B}{kT}. \tag{6}$$

Fig. 5 (curve 4) shows the Richardson plot for M100 in the temperature ranges where the TE current is expected. Φ_{BR}^0 and A_R^* that have been obtained by linear approximation are presented in Table I. It should be noted that the calculated A_R^* is much greater than the known value of 112 A $\cdot$ cm^{-2}K^{-2}.

The discrepancy between the predicted and experimentally observed SBH temperature dependences for the TE case are attributed to the interface inhomogeneity [31] and can be avoided by considering SBH under flat band condition Φ_B^{FB} [16], [31]

$$\Phi_B^{FB} = n\Phi_B^{TE} - (n-1)V_n \tag{7}$$

where $V_n = (kT/q)\ln(N_c/N_d)$ is the bulk potential, N_c is the effective density of states near the bottom of conduction band. Fig. 4(b) shows the temperature dependences of Φ_{B1}^{FB} obtained

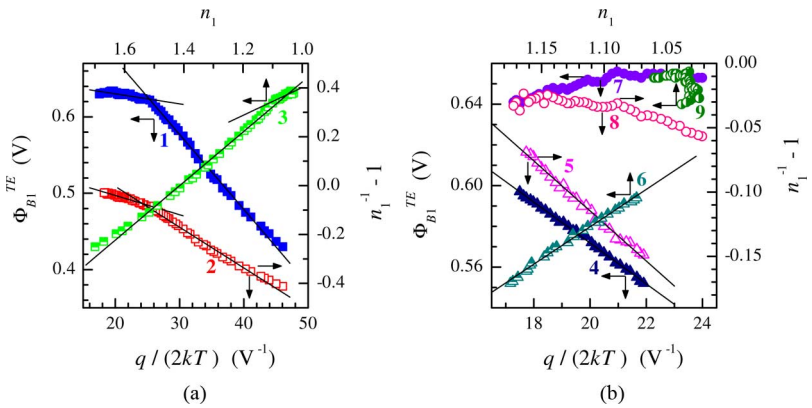

Fig. 6. Zero bias Schottky barrier height (1, 4, 7) and $(n_1^{-1}-1)$ (2, 5, 8) versus $q/(2kT)$ curves and the dependences of Schottky barrier height on ideality factor (3, 6, 9). All curves are for the main current component. D_γ, kGy: 0 (1–3), 10 (4–6), 100 (7–9). The marks are the experimental results, the lines are the least-squares linear fitting. The fitting of M0 data is carried out in temperature ranges 120–220 K and 230–330 K separately.

TABLE I
PARAMETERS DETERMINED FROM *I-V* CHARACTERISTICS OF Mo/*n*-Si STRUCTURES BY USING TE TEORY

Sample	M0		M10	M100
D_γ(kGy)	0		10	100
Temperature range (K)	120–220	230–330	260–330	260–330
σ_Φ (mV)	99 ± 1	40 ± 5	100 ± 1	–
ρ_2, 10^{-2}	33 ± 1	12 ± 1	27 ± 1	–
ρ_3 (mV)	17.0 ± 0.3	8.0 ± 0.3	19.0 ± 0.4	–
Φ_{BT}^0 (mV)	872 ± 4	663 ± 3	772 ± 2	–
Φ_{BR}^0 (mV)	872 ± 3	662 ± 3	772 ± 2	710 ± 3
A_R^* (A·cm^{-2}K^{-2})	122 ± 20	112 ± 20	115 ± 20	1200 ± 300

for the main current component. Since Φ_{B1}^{FB} and E_g display similar behavior of temperature dependences, the TE over inhomogeneous SB can be a suitable mechanism for M0 sample in the whole temperature range and for M10 sample at $T > 260$ K.

B. Thermionic Emission Over Inhomogeneous Barrier

The temperature dependences of Φ_B^{TE} and n for the case of TE current through the barrier with Gaussian distribution of height are the following [22]:

$$\Phi_B^{TE} = \Phi_B^0 - \frac{q\sigma_\Phi^2}{2kT} \tag{8}$$

$$(n^{-1}-1) = \rho_2 - \frac{q\rho_3}{2kT} \tag{9}$$

where Φ_B^0 is the mean value of SBH, σ_Φ is the SBH standard deviation, ρ_2 and ρ_3 are the coefficients that quantify voltage deformation of SBH distribution. As seen on Fig. 6, the dependences of Φ_{B1}^{TE} (curves 1 and 4) and n_1 (curves 2 and 5) on the inverse temperature are straighter for M0 and M10 (at $T > 260$ K). We note that the plots for M0 correspond to the two different lines with a transition at about 225 K, which is similar to the previously reported results [17]–[19]. The parameters Φ_{BT}^0, σ_Φ, ρ_2 and ρ_3 obtained by linear fitting of the curves in Fig. 6 for M0 and M10 are presented in Table I. It should be noted that $\Phi_{BT}^0 = 0.87$ V has been obtained for M0 in the low temperature range and is close enough to the expected value in the Bardeen limit: $\Phi_{BB} = (0.82 \pm 0.36)$ V[25], which indicates a high interface density of states.

According to the model of inhomogeneous contact with patchwork regions, the dependence of Φ_B^{TE} on n should be linear [16], [17], [23]. And the plots observed for M0 and M10 samples are linear indeed (see Fig. 6, curves 3 and 6). Moreover, two different lines are observed on Φ_B^{TE} plotted vs n, Φ_B^{TE} vs $(kT)^{-1}$ and n vs $(kT)^{-1}$ for M0 at the same temperatures. It should be noted that for M100 the classical TE mechanism is supposed and all the plots in Fig. 6 (curves 7–9) are not linear.

According to [20], [21], (8) must also be valid for the case of patches, and in this case Φ_B^0 is the SBH outside patches and σ_Φ deals with the distribution of patch parameters. Besides, if patches have different parameters, the ideality factor temperature dependence can be described by (5) and

$$T_0 = \frac{q\sigma_\Phi^2}{3kV_{bb}} \tag{10}$$

where $V_{bb} = \Phi_B^0 - V_n - V$. The value $T_{0teor} \simeq 11$ K was calculated by using (10), $V_{bb} \simeq 0.53$ V, $\Phi_{BT}^0 \simeq 0.663$ V and $\sigma_\Phi \simeq 0.04$ V. The experimental temperature dependence of n_1 for M0 sample at 230–330 K is approximated satisfactorily by (5) also yields value of $T_{0exp} \simeq 12$ K (see Fig. 2, curve 1) which is close to T_{0teor}. The dependence of n_1 vs T observed for M0 in a lower temperature range can also be caused, according to [23], by the patches.

In addition, the modified Richardson plot $F_2 = \ln(I_S/T^2) - q^2\sigma_\Phi^2/2k^2T^2$ versus $(kT)^{-1}$ is used for inhomogeneous contact [17], [18]:

$$F_2 = \ln\left(\frac{I_S}{T^2}\right) - \frac{q^2\sigma_\Phi^2}{2k^2T^2} = \ln(AA^*) - \frac{q\Phi_B^0}{kT}. \tag{11}$$

The modified Richardson plots for M0 and M10 are shown in Fig. 5 in the temperature ranges where TE current is expected. The obtained Φ_{BR}^0 and A_R^* are presented in Table I. It is necessary to note that these values of Richardson constant for M0 and M10 are very close to 112 A $\cdot$ cm^{-2}K^{-2} for n-Si reported in [27].

Thus, we have obtained several experimental evidences that the main current component in M10 at $T > 260$ K and M0 is controlled by the TE through inhomogeneous barrier.

It should be emphasized, that according to Table I, Φ_B^0 increases after a small dose of γ–irradiation; while further increase in dose leads to Φ_B^0 decrease. This result coincides with the SBH dose dependence reported in [10], [13], [14]and does not coincide with Φ_B^{TE} data obtained from *I-V* characteristics in a direct way (Fig. 4).

The slope change of the Φ_B and n versus $(kT)^{-1}$ plots has been previously interpreted as due to a significant contribution of all the other carrier transport mechanisms (TFE, DAT, recombination and generation, leakage,) except of TE at low temperature [17]–[19]. What, in our opinion, makes the TE theory applicable to M0 is the coincidence between experimentally and theoretically obtained values of the effective Richardson constant. Thus, the factor that makes the slope in Fig. 6(a) change can be an increase in electron emission rate by defects at the MS interface. Indeed, the depletion of certain defect levels at ~ 225 K should lead to the SBH decrease. Besides this, a number of patches located near larger concentrations of such defects transform into the regions where current cannot pass easily due to effective capturing the drifting electrons by traps. As a result, in a high-temperature range, σ_Φ should be smaller, which has been observed experimentally (Table I, M0 data).

The appearance of the additional current component at low temperature also can be explained by the TE over inhomogeneous barrier because, according to [23], the carriers pass through patches mainly at low temperature. It is expected that *I-V* characteristic of additional current will be significantly affected by the series resistance (see Fig. 6 in [23]). A similar behavior has been observed in our experiments (Fig. 1). If additional current is due to TE mechanism, then [16], [23]

$$I_S = f_p A A^* T^2 \exp\left[-\frac{q\Phi_{B,p}}{kT}\right] \tag{12}$$

where f_p is the coefficient introduced to estimate the effective area of patches, $\Phi_{B,p}$ is the barrier height in the patch region. The comparison of (3) and (12) allows us to find the relationship between $\Phi_{B,p}$ and Φ_B^{TE}

$$\Phi_B^{TE} = \Phi_{B,p} - \left(\frac{kT}{q}\right)\ln f_p. \tag{13}$$

Inset in Fig. 5 shows the temperature dependences of Φ_{B2}^{TE} for the additional current component. It can be seen that for all the samples these dependences are straight lines. The values of $\Phi_{B,p} = (54 \pm 4)$ mV, $f_p = (8 \pm 1) \times 10^{-13}$ for M0 and $\Phi_{B,p} = (74 \pm 6)$ mV, $f_p = (8 \pm 1) \times 10^{-13}$ for M10 were obtained by linear fitting of the experimental data. The coincidence between the experimental plot of n_2 vs T with the plot calculated by using (5) (Fig. 2, curve 4) also prove the TE character of the additional current component.

The TE mechanism cannot be used, however, in case of M100 sample in which the value of $\Phi_{B,p}$ has been found negative $\approx (-9)$ mV.

C. Thermal Field Emission

In case when current transport obeys the TFE theory, the ideality factor as well as the relationship between the saturation current and SBH at zero bias Φ_B^{TFE} can be described in the following way [24], [33]:

$$n_{tun} = \left[\frac{E_{00}}{(kT)}\right]\coth\left[\frac{E_{00}}{(kT)}\right] \tag{14}$$

$$I_S = \frac{A^* T\sqrt{\pi E_{00}(\Phi_B^{TFE} - V_n)}}{k\cosh[\frac{E_{00}}{kT}]} \times \exp\left[-\frac{V_n}{kT} - \frac{(\Phi_B^{TFE} - V_n)}{n_{tun}kT}\right] \tag{15}$$

where E_{00} is the characteristic tunneling energy. Fig. 2 presents several dependences calculated by (14). As seen from the figure, the experimental temperature dependences of n_1 for M10 in the temperature range of 120–240 K, n_1 for M100 at $T < 130$ K and n_2 for M100 are in good agreement with the dependences predicted by (14) with E_{00} equal 17.8, 23.5 and 80 meV respectively. On the other hand, in terms of TFE theory $E_{00}^{TFE} = (h/4\pi)(N_d/m^*\varepsilon\varepsilon_s)^{1/2}$ where m^* is the effective mass of the electron. E_{00}^{TFE} is equal to about 2 meV for the investigated samples and is far from the experimentally obtained E_{00} value.

The comparison of the temperature dependence of Φ_{B1}^{TFE} obtained by TFE fitting of M10 *I-V* characteristics in Fig. 4 (curve 4) shows that dependence is far from that of E_g.

Hence, the TFE mechanism cannot be applied to the main and additional current in the structure under study.

D. Defect-Assisted Tunneling

In case when current transport is controlled by multi-step DAT processes, the value of I_S should be given by [34]

$$I_S = I_{S0}\exp(\chi T) \tag{16}$$

$$\chi = \frac{\left[\beta + k\ln\left(\frac{N_c}{N_d}\right)\right]}{E_{00}} \tag{17}$$

where I_{S0} depends on the defect concentration in particular, β is the temperature coefficient of Φ_B decrease. For ideality factor (14) should be valid.

Using (17), $\beta = 0.26$ meV /K [29], [34] and E_{00} obtained from the plots of n versus T (Fig. 2), we have calculated χ_{calc} for M10 and M100 which are presented in Table II. The table also shows the values of χ_{fit} obtained by fitting the temperature dependences of I_S by using (16) (Fig. 3). As seen from the table, the set of χ_{fit} is close to the set of χ_{calc}. This fact as well as temperature dependences of I_S and n prove that the main current component for M10 at $T = 120 \div 240$ K, the main current component for M100 at $T < 130$ K and the additional current component for M100 are controlled by multi-step DAT.

E. Reverse Current

We have also analyzed the temperature dependence of the reverse current I_R at constant biases V_R. Taking into account

TABLE II
PARAMETERS DETERMINED FROM *I-V* CHARACTERISTICS OF Mo/*n*-Si STRUCTURES BY USING DAT TEORY

Sample	M10 [a]	M100 [a]	M100 [b]
D_γ(kGy)	10	100	100
Temperature (K)	120–240	110–130	110–210
E_{00} (mV)	17.8 ± 0.5	23.5 ± 0.5	80 ± 10
χ_{calc}, (10^{-3} K^{-1})	39 ± 3	26 ± 2	8 ± 1
χ_{fit}, (10^{-3}K^{-1})	73 ± 6	42 ± 4	8 ± 1
I_{S0} (10^{-14}A)	5 ± 0.5	13 ± 3	$(17 \pm 2) \cdot 10^5$

[a] for main current component.
[b] for additional current component.

the possibility of different current-transport mechanisms for different temperature ranges, we used the following equation to fit the experimental data:

$$I_R(T, V_R = const) = I_{R,0} + I_{R,I}(T) + I_{R,II}(T) = I_{R,0} + C_I T^2 \exp\left[-\frac{E_R}{kT}\right] + C_{II} \exp(\alpha T), \quad (18)$$

where $I_{R,0}$ is the temperature-independent reverse current component; $I_{R,I} = C_I T^2 \exp[-E_R/(kT)]$ is the TE current (characteristic energy E_R is connected with SBH); $I_{R,II}$ is the current caused by non-TE the mechanisms; C_I, C_{II} and α are the temperature-independent constants. The value used for non-irradiated sample is $I_{R,II} = 0$ and the other addents for M0 have been approxmated for two separate ranges: 120–220 K and 230–330 K.

Fig. 7 presents the temperature dependences of the component relative contribution $I_{R,j}/I_R$ ($j = 0, I, II$) for a certain value of V_R. It can be seen that $I_{R,0}$ contribution increases with temperature decrease and the reverse bias increases being the greatest for M 100. $I_{R,I}$ is dominant for M0 at low bias ($V_R = 0.5$ V) at almost all the temperatures. $I_{R,II}$ exceeds the TE current ($I_{R,I}$) for M10 at $T < 240$ K and this coincides with the result based on the forward current analysis. $I_{R,I}$ contribution for M100 becomes prevailing at $T > 300$ K only, whereas at a lower temperature the temperature-independent component is dominant.

Fig. 8 shows field dependences of $I_{R,0}$ in the Fowler-Nordheim coordinates: $\ln(I_{R,0}/E_m^2)$ versus $1/E_m$, where $E_m = (2qN_d V_{bb}/\varepsilon_s)^{1/2}$ is the electric field at the MS interface [24], [25]. The obtained values of Φ^0_{BR} and V_n at $T = 250$ K have been used to calculate E_m. The linearity of the dependences as well as that $I_{R,0}$ does not depend on temperature testify to the tunneling nature of this component. In case of tunneling across triangular barrier, the modified Fowler-Nordheim equation can be used [25], [36]

$$\ln\left(\frac{I_{R,0}}{E_m^2}\right) \propto -\frac{8\pi\sqrt{2m^*}(q\Phi_{FN})^{3/2}}{3hqE_m} \quad (19)$$

where Φ_{FN} is approximately equal to the energy depth of the level in tunneling through the deep center. The value $\Phi_{FN} = (120 \pm 5)$ mV has been obtained for all the samples by using

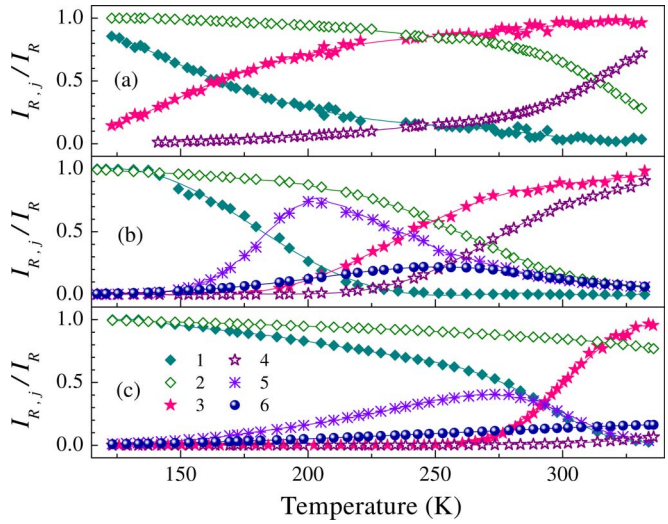

Fig. 7. The temperature dependences of relative contribution of the reverse current component $I_{R,0}$ (1, 2), $I_{R,I}$ (3, 4), and $I_{R,II}$ (5, 6). V_R, V: 0.5 (1, 3, 5), 3 (2, 4, 6). D_γ, kGy: 0 (a), 10 (b), 100 (c).

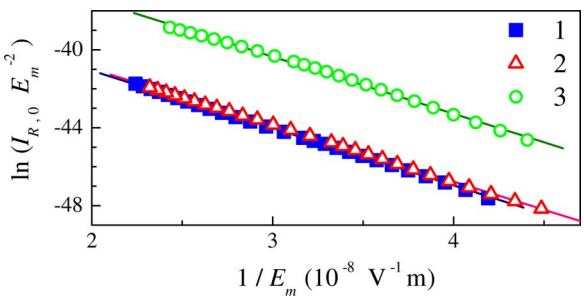

Fig. 8. The Fowler-Nordheim plots of the temperature-independent component of the reverse current. D_γ, kGy: 0 (1), 10 (2), 100 (3). The lines are the least-squares linear fitting.

linear fitting of the data in Fig. 8. The obtained value is close to the acceptor level of the interstitial carbon ($E_c - (0.10 \div 0.12)$ eV). And this center is typical defect in γ-irradiated silicon.

It is necessary to emphasize the following: i) the tunneling component prevails for M100 reverse current at almost all the biases and temperatures [see Fig. 7(c)]; ii) the temperature dependence of the main component saturation current is weak at 150–220 K [see Fig. 3(a), curve 3]. In our opinion, these facts prove the tunneling mechanism of the forward main current component for M100 at the same temperature. Additionally the presence of the tunneling component is shown to cause errors in SBH and A^* determined by using the Richardson plot [37]. We believe that the influence of tunneling mechanism remains essential for M100 sample in the temperature range 260–330 K, and for this reason the obtained (Table I) and known value of Richardson constant are different.

The experimentally observed dependence of E_R on V_R indicates the change of the barrier height. It is known [23], [24], [38] that such SBH lowering (and "soft" reverse characteristics) may occur due to the image force (in this case SBH variation $\Delta\Phi_B \sim {V_R}^{1/4}$), the electric field ($\Delta\Phi_B \sim {V_R}^{1/2}$) and the patches. In case when the patches are not equal, $\Delta\Phi_B \sim {V_R}^{2/3}$ and the proportionality factor depends on the patch parameters

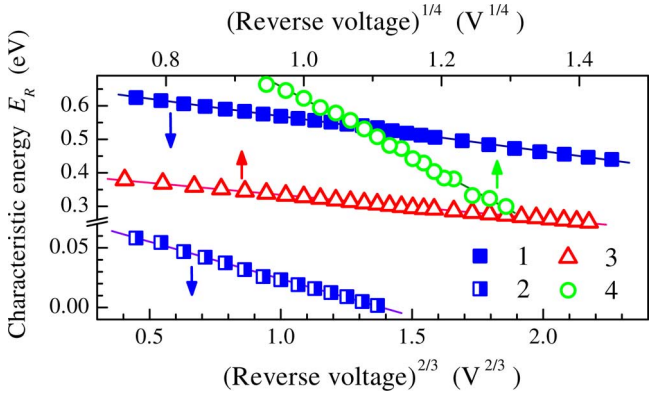

Fig. 9. The Fowler-Nordheim plots of the temperature-independent component of the reverse current. D_γ, kGy: 0 (1), 10 (2), 100 (3). The lines are the least-squares linear fitting.

[23]. The data presented in Fig. 9 demonstrate the linear dependence between E_R and $V_R^{2/3}$ for M0 in both temperature ranges. It is an additional argument for the applicability of the patch model and for patch's parameters changing at $\simeq 225$ K. In M10 and M100 the SBH lowering is controlled by the image force (see Fig. 9).

To summing up, the main current component in non-irradiated Mo/n-Si Schottky structure is controlled by TE over Schottky contact with patch regions. The mean SBH Φ_B^0 and SBH standard deviation σ_Φ are 872 mV and 0.099 V in 120–220 K range, and 663 mV and 0.040 V in 230–330 K range, respectively. The recharge of some interface defects in the at $T \simeq 225$ K leads to decrease both in SBH and in the fraction of patches involved in the charge transfer. The additional current observed at low temperature ($T < 220$ K) and small bias ($V < 0.2$ V) is due to TE processes that occur only in the patch regions. The reverse current is controlled by TE and tunneling, the latter becoming more important as the temperature decreases or the bias increases.

After the structures were exposed to ^{60}Co γ-rays radiation of $D_\gamma = 10$ kGy, the DAT with characteristic tunneling energy $E_{00} = 17.8$ meV becomes prevailing in the temperature range 120–240 K both at forward and reverse bias. The TE over inhomogeneous barrier with $\Phi_B^0 = 772$ mV and $\sigma_\Phi = 0.1$ V is the main current-generating process at $T > 260$ K. The SBH in the homogeneous region and the standard deviation of the patch parameters are greater than those in the non-irradiated structure at the same temperature. In our opinion, this can be attributed to irradiation-induced defects in the depletion region, which leads to the increase of the band gap level concentration and enhancement of DAT. Moreover, the acceptor defects accumulate at MS interface causing a slight decrease of N_d and increase of Φ_B^0 B and σ_Φ. It should be noted that the spatial separation of oppositely charged γ-ray induced defects can be caused by the elastic field in the barrier structyres [39], [40]. The enhanced influence of patches masks the growth of SBH in the homogeneous region and leads to the effective drop of SBH, which is determined from *I-V* characteristic. The additional forward current which is observed at low-temperatures can be related to the TE occurring in the patch regions. It should be noted that the study of additional current component show that the patched area do not change after irradiation whereas the barrier height increases (from 54 to 74 mV). This can be explained by hypothesizing that interface acceptor concentration increases as well.

The additional current increases significantly with the dose up to 100 kGy and its transport mechanism changes from TE to DAT with $E_{00} = 80$ meV. Besides that, the tunneling current becomes the major contributor not only at reverse bias in practically the entire temperature range but also at forward bias at $T = 150 \div 220$ K. The forward current in 260–330 K range is mainly controlled by TE over 710 mV Schottky barrier although the influence of tunneling also should not be neglected. It is known [41] that the defect gettering can take place in SD under the action of high-energy photon, which results in relaxation of existing mechanical stresses. In our opinion, in the samples under study the gettering centers are patches. As a consequence, SBH and the accumulated negative charge decrease in the homogeneous region (Table I). Moreover, the patches turn into shunt regions with tunneling charge-transport mechanism. Since the patches stop affecting the TE processes the effective SBH, which is obtained from *I-V* characteristic, increases in comparison with $D_\gamma = 10$ kGy samples contrary to the SBH reduction at the homogeneous region.

It is necessary to note that both non-monotonic change of the mechanical stress in epitaxial films and alteration of the charge sign of the radiation defects accumulating at the interface with the ^{60}Co γ-rays dose increase have been observed [40], [42]. These effects as well indirectly support the proposed mechanism.

IV. Conclusion

The experimental investigation of Mo/n-Si Schottky barrier structure irradiated by ^{60}Co γ–rays has been carried out. The investigation has shown that irradiation significantly enhances the tunneling current at forward and reverse bias. It has been found that the tunneling process and thermionic emission are the dominant forward current transport mechanisms for the irradiated structures at $T < 250$ K and $T > 260$ K respectively. In non-irradiated structure however, the forward current is controlled by thermionic emission only. The Schottky doide parameter modification has been demonstrated to have different nature in the samples with low and high ^{60}Co γ–rays cumulative dose. In particular, at a low dose, the influence of patches on forward current increases in the inhomogeneous barrier structures, whereas at a high dose this effect completely disappears. The barrier height, ideality factor, and reverse current have been found to depend non-monotonically on the cumulative dose. The behavior of the non-monotonic dependence of barrier height is supposed to be different for inhomogeneous and homogeneous barrier structures. The obtained results can be used to modify MS structure parameters.

References

[1] S. Kumar, Y. S. Katharria, Y. Batra, and D. Kanjilal, "Influence of swift heavy ion irradiation on electrical characteristics of Au/n-Si (100) Schottky barrier structure," *J. Phys. D, Appl. Phys.*, vol. 40, no. 22, pp. 6892–6897, Nov. 2007.

[2] S. Kumar, Y. S. Katharria, and D. Kanjilal, "Swift heavy ion irradiation-induced defects and electrical characteristics of Au/n-Si Schottky structure," *J. Phys. D, Appl. Phys.*, vol. 41, no. 10, p. 105105, May 2008.

[3] A. Rao, S. Krishnan, G. Sanjeev, and K. Siddappa, "Effect of 8 MeV electrons on Au/n-Si Schottky diodes," *Int. J. Pure Appl. Phys.*, vol. 5, no. 1, pp. 55–62, 2009.

[4] A. T. Sharma *et al.*, "In-situ current-voltage analysis of Au/GaAs Schottky diode under nitrogen ion irradiation," *Surf. Coat. Technol.*, vol. 203, no. 17–18, pp. 2667–2669, Jun. 2009.

[5] H. Ohyama *et al.*, "Radiation damage of SiC Schottky diodes by electron irradiation," *J. Mater. Sci.: Mater. Electron.*, vol. 16, no. 7, pp. 455–458, Jul. 2005.

[6] A. Tataroglu, S. Altindal, and M. M. Bulbul, "^{60}Co γ irradiation effects on the current-voltage *(I-V)* characteristics of Al/SiO_2/p-Si (MIS) Schottky diodes," *Nucl. Instrum. Meth. Phys. Res. A*, vol. 568, no. 2, pp. 863–868, Dec. 2006.

[7] I. Tascioglu, A. Tataroglu, A. Ozbay, and S. Altindal, "The role of ^{60}Co γ-ray irradiation on the interface states and series resistance in MIS structures," *Radiat. Phys. Chem.*, vol. 79, no. 4, pp. 457–461, Apr. 2010.

[8] A. Tataroglu and S. Altindal, "Analysis of interface states and series resistance at MIS structure irradiated under ^{60}Co γ-rays," *Nucl. Instrum. Meth. Phys. Res. A*, vol. 580, no. 3, pp. 1588–1593, Oct. 2007.

[9] A. Tataroglu and S. Altindal, "Electrical characteristics of ^{60}Co γ-ray irradiated MIS Schottky diodes," *Nucl. Instrum. Meth. Phys. Res. B*, vol. 252, no. 2, pp. 257–262, Nov. 2006.

[10] S. Karatas and A. Turut, "Electrical properties of Sn/p-Si (MS) Schottky barrier diodes to be exposed to ^{60}Co γ-ray source," *Nucl. Instrum. Meth. Phys. Res. A*, vol. 566, no. 2, pp. 584–589, Oct. 2006.

[11] G. A. Umana-Membreno *et al.*, "Annealing of ^{60}Co gamma radiation-induced damage in n-GaN Schottky barrier diodes," *J. Appl. Phys.*, vol. 101, no. 5, p. 054511, Mar. 2007.

[12] A. Kinoshita *et al.*, "Radiation effect on pn-SiC diode as a detector," *Nucl. Instrum. Meth. Phys. Res. A*, vol. 541, no. 1–2, pp. 213–220, Apr. 2005.

[13] G. I. Vorobets, M. M. Vorobets, V. N. Strebezhev, E. V. Buzaneva, and A. G. Shkavro, "Physical mechanisms of laser correction and stabilization of the parameters of Al-n-n^+-Si-Al Schottky barrier structures," *Semiconductors*, vol. 38, no. 6, pp. 663–665, Jun. 2004.

[14] M. Pattabi, S. Krishnan, and G. X. Mathew, "Effect of temperature and electron irradiation on the *I-V* characteristics of Au/CdTe Schottky diodes," *Sol. Energy*, vol. 81, no. 1, pp. 111–116, Jan. 2007.

[15] Z. D. Kovalyuk *et al.*, "The effect of neutron radiation on the photoelectric parameters of ITO-GaSe structures," *Semiconductors*, vol. 41, no. 5, pp. 550–554, May 2007.

[16] K. Sarpatwari, S. E. Mohney, and O. O. Awadelkarim, "Effects of barrier height inhomogeneities on the determination of the Richardson constant," *J. Appl. Phys.*, vol. 109, no. 1, p. 014510, Jan. 2011.

[17] I. Tascioglu, U. Aydemir, and S. Altindal, "The explanation of barrier height inhomogeneities in Au/n-Si Schottky barrier diodes with organic thin interfacial layer," *J. Appl. Phys.*, vol. 108, no. 6, p. 064506, Sep. 2010.

[18] N. Yildirim, K. Ejderha, and A. Turut, "On temperature-dependent experimental *I-V* and *C-V* data of Ni/n-GaN Schottky contacts," *J. Appl. Phys.*, vol. 108, no. 11, p. 114506, Dec. 2010.

[19] M. Mamor, "Interface gap states and Schottky barrier inhomogeneity at metal/n-type GaN Schottky contacts," *J. Phys.: Condens. Matter*, vol. 21, no. 33, p. 335802, Aug. 2009.

[20] F. Iucolano, F. Roccaforte, F. Giannazzo, and V. Raineri, "Barrier inhomogeneity and electrical properties of Pt/GaN Schottky contacts," *J. Appl. Phys*, vol. 102, no. 11, p. 113701, Dec. 2007.

[21] F. Iucolano, F. Roccaforte, F. Giannazzo, and V. Raineri, "Temperature behavior of inhomogeneous Pt/GaN Schottky contacts," *Appl. Phys. Lett.*, vol. 90, no. 9, p. 092119, Feb. 2007.

[22] J. H. Werner and H. H. Guttler, "Barrier inhomogeneities at Schottky contacts," *J. Appl. Phys.*, vol. 69, no. 3, pp. 1522–1533, Feb. 1991.

[23] R. T. Tung, "Electron transport at metal-semiconductor interfaces: General theory," *Phys. Rev. B*, vol. 45, no. 23, pp. 13509–13523, Jun. 1992.

[24] E. H. Rhoderick and R. H. Williams, *Metal Semiconductor Contacts*. : Oxford: Clarendon, 1988.

[25] S. M. Sze, *Semiconductor Devices: Physics and Technology*. NewYork: Wiley, 1985.

[26] D. Gromov and V. Pugachevich, "Modified methods for the calculation of real Schottky-diode parameters," *Appl. Phys. A*, vol. 59, no. 3, pp. 331–333, Sep. 1994.

[27] D. K. Schroder, *Semiconductor Material and Device Characterization*. Hoboken, NJ: Wiley, 2006, p. 158.

[28] S. Zhu *et al.*, "A BEEM study of the temperature dependence of the barrier height distribution in PtSi/n-Si Schottky diodes," *Sol. St. Com.*, vol. 112, no. 11, pp. 611–615, Oct. 1999.

[29] M. O. Aboelfotoh, "Electrical characteristics of W-Si(100) Schottky barrier junctions," *J. Appl. Phys.*, vol. 66, no. 1, pp. 262–72, Jul. 1989.

[30] T. Markvart and L. Castaner, *Practical Handbook of Photovoltaics. Fundamentals and Application*. New York: Elsevier, 2003, pp. 98–99.

[31] I. Dokme, S. Altindal, and I. M. Afandiyeva, "The distribution of the barrier height in Al-TiW-Pd_2Si/n-Si Schottky diodes from *I-V-T* measurements," *Semicond. Sci. Technol.*, vol. 23, no. 3, p. 035003, Mar. 2008.

[32] R. F. Schmitsdorf, T. U. Kampen, and W. Mönch, "Explanation of the linear correlation between barrier heights and ideality factors of real metal-semiconductor contacts by laterally nonuniform Schottky barriers," *J. Vac. Sci. Technol. B*, vol. 15, no. 4, pp. 1221–1226, Jul. 1997.

[33] B. Roul *et al.*, "Temperature dependent electrical transport behavior of InN/GaN heterostructure based Schottky diodes," *J. Appl. Phys.*, vol. 109, no. 4, p. 044502, Feb. 2011.

[34] V. V. Evstropov, Y. V. Zhilyaev, M. Dzhumaeva, and N. Nazarov, "Tunnel excess current in nondegenerate barrier ($p-n$ and $m-s$) silicon-containing III-V structures," *Semiconductors*, vol. 31, no. 2, pp. 115–120, Feb. 1997.

[35] A. A. Evtukh, E. B. Kaganovich, E. G. Manoilov, and N. A. Semenenko, "A mechanism of charge transport in electroluminescent structures consisting of porous silicon and single-crystal silicon," *Semiconductors*, vol. 40, no. 2, pp. 175–179, Feb. 2006.

[36] Y. N. Novikov, "Non-volatile memory based on silicon nanoclusters," *Semiconductors*, vol. 43, no. 8, pp. 1040–1045, Aug. 2009.

[37] L. S. Yu *et al.*, "The role of the tunneling component in the current-voltage characteristics of metal-GaN Schottky diodes," *J. Appl. Phys.*, vol. 84, no. 4, pp. 2099–2104, Aug. 1998.

[38] J. M. Andrews and M. P. Lepselter, "Reverse current-voltage characteristics of metal-silicide Schottky diodes," *Sol.-St. Elect.*, vol. 13, no. 7, pp. 1011–1023, Jul. 1970.

[39] K. D. Shcherbachev, V. T. Bublik, V. N. Mordkovich, and D. M. Pazhin, "Specific features of formation of radiation defects in the silicon layer in silicon-on-insulator structures," *Semiconductors*, vol. 45, no. 6, pp. 738–742, Jun. 2011.

[40] S. A. Muzafarova, S. A. Mirsagatov, and F. N. Dzhamalov, "Effect of irradiation with gamma-ray photons on the charge-transport mechanism in n-CdS/ p-CdTe heterostructures," *Semiconductors*, vol. 43, no. 2, pp. 175–80, Feb. 2009.

[41] N. S. Boltovets *et al.*, "Microwave-stimulated relaxation of internal strains in GaAs-based device heterostructures," *Tech. Phys. Lett.*, vol. 28, no. 2, pp. 154–156, Feb. 2002.

[42] A. E. Belyaev *et al.*, "Electroreflectance study of the effect of γ radiation on the optical properties of epitaxial GaN films," *Semiconductors*, vol. 46, no. 3, pp. 302–305, Mar. 2012.